Application of a Scattered-Light Radiometric Power Meter

James N. Caron,[1] Gregory P. DiComo,[1] Antonio C. Ting,[2] and Richard P. Fischer[2]

[1] *Research Support Instruments, 4325-B Forbes Boulevard, Lanham, MD 20706*[a]

[2] *Naval Research Laboratory, 4555 Overlook Ave., S.W., Washington, DC 20375-5337*

(Dated: 4 April 2011)

The power measurement of high-power continuous-wave laser beams typically calls for the use of water-cooled thermopile power meters. Large thermopile meters have slow response times that can prove insufficient to conduct certain tests, such as determining the influence of atmospheric turbulence on transmitted beam power. To achieve faster response times, we calibrated a digital camera to measure the power level as the optical beam is projected onto a white surface. This scattered-light radiometric power meter saves the expense of purchasing a large area power meter and the required water cooling. In addition, the system can report the power distribution, changes in the position, and the spot size of the beam. This paper presents the theory of the scattered-light radiometric power meter and demonstrates its use during a field test at a 2.2 km optical range.

---

[a] Electronic mail: Caron@RSImd.com

I. INTRODUCTION

For continuous-wave high-power laser experiments, there are significant disadvantages in measuring the power with a conventional thermopile power meter.[1–3] These meters are not inexpensive, require active water cooling units, and have slow response times. For example, the response time of a 20-cm diameter thermopile meter can exceed 40 seconds. Alternatively, a digital video camera can be used to capture the image of the laser spot on a suitable imaging surface. This provides qualitative information about the power and profile of the laser spot. With calibration, the imaging system can provide quantitative power measurements at a rate limited by the frame rate of the camera. In addition, the camera produces spatial information, such as power distribution and spot size, which cannot be acquired using a power meter alone.

The scattered-light radiometric power meter consists of an imaging surface, a digital video camera with computer interface, and appropriate optics. For the imaging surface, we employ a quarter-inch thick plate of Macor, a machinable glass ceramic developed by Corning Incorporated.[4] Macor has diffuse reflection, low thermal conductivity, and can be heated to 1000° C making it useful for laser cavity components.[5] This method was developed for testing the propagation of continuous-wave high-power laser beams through atmospheric turbulence.[6,7]

II. THEORY

The system model, shown in Figure 1, consists of a laser beam with power P_o impinging an imaging surface, resulting in a scattered power of $R\Theta P_{ip}$ where R is the reflectivity of the surface at the laser wavelength, and P_{ip} is the power on the imaging surface in an area equal to the projection of a pixel. The power radiates into a hemisphere of area $2\pi d_L^2$ where d_L is the distance to the camera lens with aperture radius of a.

The parameter Θ is the angular dependence for the received light, being a function of the angle of the incoming laser light θ, the viewing angle ϕ and the level of specular reflection of the imaging screen. This is a simplification of the bidirectional reflectance distribution function (BRDF) used to describe the relationship between the reflected radiance and incident irradiance of a surface.[8] If the BRDF is known, as it is with many materials used in

optics experiments, then Θ can be derived from the BRDF.

The power that falls on the lens through a filter with transmission of T_f is

$$P_{lens} = T_f R\Theta P_{ip} \frac{\pi a^2 cos\varphi}{2\pi d_L^2} = \frac{a^2 T_f R\Theta P_{ip} cos\varphi}{2d_L^2} \tag{1}$$

where φ is the angle between the optical axis of the lens and the ray that extends from the center of the lens to the imaged point on the image plane. Assuming the laser spot is centered in the image, the angle φ can be calculated from

$$\cos\varphi = \frac{f}{\sqrt{f^2 + p^2(m^2 + n^2)}} \tag{2}$$

where p is the pixel size, m and n are the image indices referenced to the central pixel, and f is the focal length of the lens. At the edge of a common focal plane array where $f = 35$ mm, $p = 4.7\mu$m, $m = 320$, and $n = 240$, the cosine factor is $\cos\varphi = 0.9986$. In most cases, the error introduced by exclusion of this factor is negligible.

With an ideal lens and focus, the power at a pixel in the focal plane is

$$P_{fp} = T_L P_{lens} = \frac{a^2 T_L T_f R\Theta P_{ip}}{2d_L^2} \tag{3}$$

where T_L is the transmission coefficient of the lens. The summation of all pixel values is proportional to the total incident laser power P_o.

To ensure accuracy, it is important to subtract off the background image produced by the combination of non-laser light and fixed-pattern noise. This is accomplished by imaging the Macor plate at the same exposure setting while the laser is not emitting. Effects such as CCD blooming, saturation, and changing light conditions can also produce inaccurate results. These artifacts can be eliminated by careful choice of filters and taking frequent background images. If the field-of-view of the camera is larger than the Macor plate, the operator should define a region-of-interest in the image such that light scattered outside of the target is not included in the measurement.

A.   Camera Parameters

This paper will use operational parameters from our system that uses a Sony XCD-V50 camera.[9] The amplification A_G of the signal by the gain setting is

$$A_G = 10^{18G/(512*20)} \tag{4}$$

where G is the camera gain setting. The exposure time t_e (in microseconds) is calculated using

$$t_e = (\text{Int}[H \times 0.64] \times 32.55) + 10 \tag{5}$$

where H is the camera shutter setting and $\text{Int}[...]$ produces an integer result.[9]

The power per pixel is proportional to the pixel amplitude as expressed in analog-digital units (ADUs), described by

$$P_{fp} = \frac{C_s I_p}{A_G t_e q_{rel}(\lambda) F} \tag{6}$$

where I_p is the ADU value of a pixel in the image after flat-fielding and background subtraction, C_s is a camera calibration factor, F is the fill fraction of the sensor, t_e is the exposure time, A_G is the camera gain, and $q_{rel}(\lambda)$ is the relative quantum efficiency of the sensor. Equating equations 3 and 6 produces

$$P_{ip} = \frac{2 d_L^2 C_s I_p}{a^2 R \Theta T_L T_f A_G t_e q_{rel}(\lambda) F}. \tag{7}$$

Another important camera characteristic is nonlinear CCD response, especially at ADU values near the saturation point. This was tested by imaging an integrating sphere with increasing exposure times until saturation was reached. The average pixel value was measured in four regions-of-interest, and are displayed in Figure 2. The slope and intercepts of the lines were calculated. These lines were extended up to the saturation point. It is quite clear from the analysis that there are no significant nonlinearities in this camera for ADU levels under 60000.

B. Angular Reflectivity

For any practical experiment involving the camera calibration, the camera must be offset from the laser optical path or else block a portion of the incoming laser light. As discussed above, this requires a measurement of the BRDF of the target material. However, we can constrain the position of the camera such that the optical axis is normal to the target board in the vertical direction. In this manner, the angular reflectivity need only be measured along the horizontal plane.

We tested the angular dependence of the reflectance of the Macor by directing a small laser onto the imaging surface. The camera was mounted on a pivot arm, keeping the camera-to-screen distance constant, but varying the view angle in the horizontal plane. To

4

prevent the camera from blocking the laser beam at the central position, the laser was positioned slightly higher than the camera. As the view angle is varied, an image is taken of the beam. The average pixel value for each position was taken, and is shown in Figure 3.

A good curve fit was achieved using the Phong model[10]

$$\Theta = C_1 \cos^n (\phi - \theta). \tag{8}$$

With measured values of ϕ and θ, a regression fit produces values of $C_1 = 0.99$ and $n = 0.99$ with a goodness-of-fit R^2 value of 0.996.

There has been published research[11] on the BRDF of Macor in the form of Accuflect.[12] However, this function is dependent on the surface roughness of the material which is dependent on how the material was machined. Therefore it is preferable to measure this quantity as opposed to relying on published reports. Macor was chosen as the target surface based on the material's diffuse surface, low cost, and high thermal stability. Other materials can be used as well. Spectralon[13] is a thermoplastic resin that is often used in the fabrication of optical test equipment. Even though the thermal stability is much lower than Macor, Spectralon is often produced with very high reflectivity. Since Spectralon has become a standard for optical calibration, several papers have been published that discuss the Spectralon BRDF.[14–16]

C. Camera Calibration

The calibration factor C_s is not usually made available by camera manufacturers, but can be determined empirically by using a light source with a known power level. In addition, many of the parameters in Equation 7 can be combined into a single system-specific calibration factor

$$C_T = \frac{2C_s}{RT_L q_{rel}(\lambda)F} \tag{9}$$

producing

$$P_{ip} = \frac{d_L^2 C_T I_p}{a^2 \Theta T_f A_G t_e}. \tag{10}$$

where the calibration factor C_T has units of Joules per ADU.

III.   APPLICATION

The method was tested in both a laboratory and field environment. The calibration was performed using a low-power infrared laser with wavelength of 1064 nm and measured power of 0.126 W. Several calibration factors were measured while making changes to the distance d_L, and averaged to produce $C_T = 1.31 \times 10^{-16}$ J/ADU.

The output of the Yb-Fiber laser was measured to be 20.0 W from a thermopile power meter rated for accuracy within 2%. With a distance d_l of 1.55 meters, an aperture radius of 15.8 mm, unity gain, exposure of 1.4 ms, and a pixel sum of 1.64×10^7 ADUs, the calculated power was 20.1 W. Saturation was avoided by inserting a heat-absorbing filter in front of the camera lens.

In the field experiment, two lasers were directed onto a one-foot square piece of Macor from a distance of 2.2 km. The measured power of Laser 1, recorded in a laboratory with a thermopile with 5% accuracy, was 18.8 W. The power of Laser 2 was recorded as 31.2 W. Six runs were performed: two runs with Laser 1; two runs with Laser 2; and two runs with both lasers on the target. Figure 4 shows images with a single beam (left) and two beams (right) on the Macor target. Figure 5 shows a comparison of the laser power as measured in the laboratory, and power measured by the scattered-light radiometric power meter after propagating down range. The run index is given by the x-axis. The estimated error in the radiometric measurements is 6.4%, produced primarily by uncertainty in the geometric measurements and the calibration faction.

The measurements are on average 13.8% less than the power produced by the lasers. This loss can be explained through several factors. First, there is a loss from the optical beam director and collimators. For propagation down range, the beams are initially down-collimated using several lenses, and reflected off a variety of mirrors before propagating down-range to the target. Each reflection contributes to the loss.

Secondly, portions of the beam can scatter off aerosols. The field tests took place during September 2009 in Albuquerque, NM over a 2.2 km horizontal path where the beam height over the surface varied from two to thirty meters. The atmospheric extinction coefficient for a similar environment[17] was estimated as 0.014 /km for wavelengths near 1 micron, resulting in 3% power loss from aerosol scattering.[18,19]

The third source of loss results when turbulent cells direct a portion of the beam off-target.

6

Figure 6 shows a plot of laser power as a function of time for the second run. Emission began at 2 seconds and ended at 18 seconds. The average power measured for this run was 16.1 W, 14.2% below the lab-measured power. The graph shows fluctuations that are on the order of 10%. The amplitude of the fluctuations increases when the effective size of the target is decreased (by decreasing the size of the region-of-interest). Visual observations of the image sequences also support that the turbulence was strong enough to move a portion of the beam off target. This was especially evident in the sixth run where higher turbulence produced a significantly lower average power.

The maximum power recorded can be used to estimate the transmission without turbulence. Similar to lucky imaging,[20] the frame that contains maximum number of ADUs in the image sequence represents a point in time where the turbulence is weakest. The maximum power recorded during the second run is 17.9 W which is only 1.9 % below the lab-measured laser power. The average of the maximum values for all runs was 1.7% below lab-measured powers with a standard deviation of 4.2%.

The dotted line in Figure 6 shows the laser spot radius as measured using the geometric mean of the x (horizontal) and y (vertical) variances. The thin line shows the distance from the averaged spot position to the instantaneous position as measured using a centroid function. Power decreases as the absolute value of the spot position increases. These measures provide information that cannot be obtained using a conventional thermopile detector and can explain power changes caused by drifting, heating of the optical components, thermal blooming, and turbulence.

Care has to be taken in processing of the images since background noise, nonlinear response, blooming, and stray light could affect the results. With correct calibration, these measurements can be taken and reported in real time, while important data such as spot position, power distribution, and spot size are also generated.

IV.   CONCLUSIONS

We have presented a scattered-light radiometric power meter that provides an alternative to thermopile or calorimetric[21,22] optical power meters. A digital camera records the laser spot as it is scattered off a Macor plate for a known geometry. The images can be processed in real time or after the experiment to produce a power measurement for each frame. In

addition to overall power, the images provide information on spot size, spot position, and regional variations of power. Validating experiments were performed both in a laboratory setting, and during the long-range test of a high-power continuous-wave laser system. Very good agreement was achieved in the laboratory setting where power was measured with both a conventional thermopile power meter and the technique discussed here. During six runs of the long-range test, the scattered-light radiometric power meter recorded powers that were 13.8% less than the power measured using a thermopile meter in a laboratory. This difference can be attributed to a combination of optical loss in the beam director, scattering from aerosols, and the redirection of the beam off of the target through interaction with turbulence.

V. ACKNOWLEDGMENTS

REFERENCES

[1] R.W. Zimmerer, U.S. Patent 4,522,511, (July 11, 1985).

[2] X. Li, T.R. Scott, C.L. Cromer, D. Keenan, F. Brandt, K. Mstl, *Metrologia*, **37**, 445 (2000).

[3] J.S. Preston, *J. Phys. E: Sci. Instrum.*, **4**, 969 (1971).

[4] Corning Incorporated, Specialty Materials, One Riverfront Plaza, Corning, NY 14831 USA.

[5] A. Krajewski and P. Mazzinghi, J. Mater. Sci. **29**(1), 232 (1994).

[6] P. Sprangle, J.R. Peano, B. Hafizi, and A.C. Ting, *Journal of Directed Energy*, **2** 3 (2007).

[7] P. Sprangle, A. Ting, J. Peano, R. Fischer, and B. Hafizi, IEEE J. Quantum Electron. **45**, 138 (2009).

[8] F. Nicodemus, Appl. Opt. **4**(7), 767 (1965).

[9] See http://www.sony.co.uk for Operators Manual of Sony Corp., 1-7-1 Konan, Minato-ku, Tokyo, Japan.

[10] B. Phong, Commun. ACM **18**(6), 311 (1975).

[11]M.R. Cohen and L. J. Small, Technical Note 3, (2003) http://www.4physics.com/tn3/lambertian.htm.

[12]See http://www.Accuratus.com for Accuratus Corporation, Phillipsburg, NJ, USA.

[13]See http://www.LabSphere.com for USA Labsphere, North Sutton, NH, USA.

[14]C. Bruegge, N. Chrien, and D. Haner, *Remote Sens. Environ.*, **76** 354 (2001).

[15]D. Mohammad, K. P. Nielsen, L. Zhao, . Frette, B. Hamre, and J. J. Stamnes, (Poster) Northern Optics, Bergen Norway, June 16-18 (2006).

[16]K. J. Voss and H. Zhang, *Appl. Opt.* **45** (30), 7924 (2006).

[17]R.T. Pinker, G. Pandithurai, B.N. Holben, T.O. Keefer, and D. Goodrich, *Atmos. Res.*, **71**, 243 (2004).

[18]L. C. Andrews and R. L. Phillips, *Laser Beam Propagation Through Random Media* (SPIE, Bellingham, Washington, 1998).

[19]S. Kato, M. H. Bergin, T. P. Ackerman, T. P. Charlock, E. E. Clothiaux, R. 296 A. Ferrare, R. N. Halthore, N. Laulainen, G. Mace, J. Michalsky, and D. D. 297 Turner, J. Geophys. Res. **105**, 14701, (2000).

[20]D. L. Fried, J. Opt. Soc. Am. 68, 1651 (1978).

[21]S.R. Gunn, *J. Phys. E: Sci. Instrum.*, **6**, 105 (1973).

[22]X. Li, J. A. Hadler, C. L.Cromer, J. H. Lehman, and M. L. Dowell, NIST Spec. Publ. **250-77**, 32697 (2007).
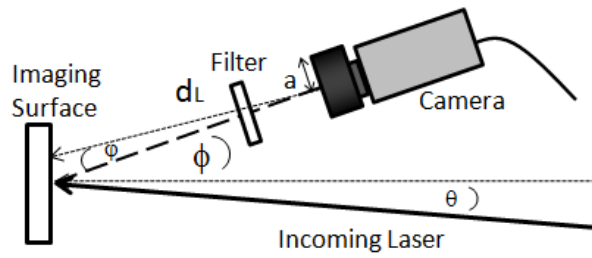
FIG. 1. Arrangement for the camera and target surface. The scattered laser light is imaged by a camera. Calibration of the camera and system geometry allows the quantitative measurement of incident laser power with a response time limited by the frame rate of the camera.
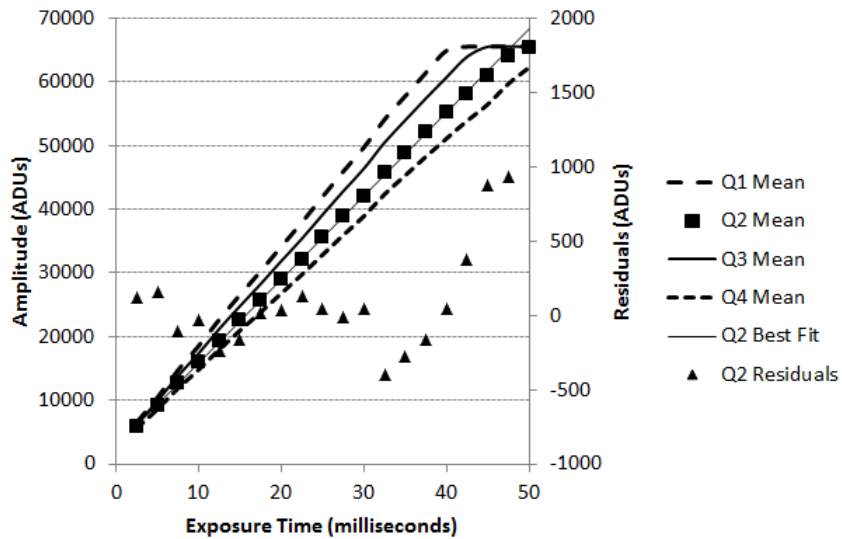

FIG. 2. The camera was tested for nonlinearities. Images of a flat field were taken as a function of exposure time. The average pixel value in each quadrant was measured and plotted. The graph also shows a line created from a regression fit from quadrant 2 and the residuals on the second Y axis. A nonlinearity can be seen near counts of 60,000 ADUs.
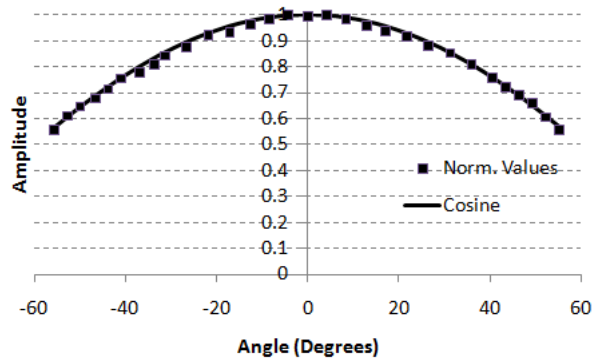
FIG. 3. The normalized dependence of the radiometric power meter on viewing angle. A camera mounted on a pivot arm imaged a laser spot from different angles. The average values, after background subtraction, of each image were recorded. The normalized averages are plotted alongside a curve fit based on the Phong model.
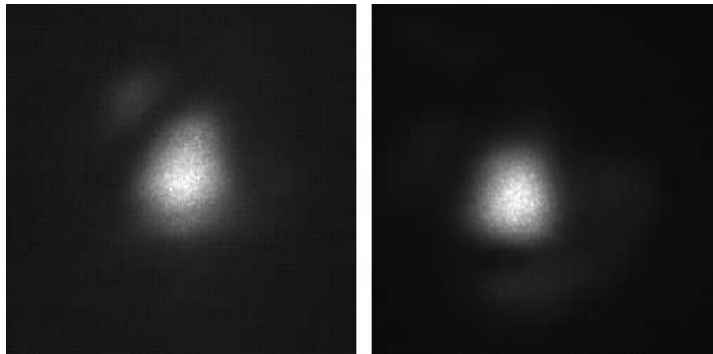

FIG. 4. Recorded images of laser beams on the Macor target from the field test. Each image has the dimension of 250×250 square pixels where the length of a pixel corresponds to 0.7 mm. The image on the left is from the second run using a single beam. The image on the right is from the last run where the two beams are aligned to the same position. The images were captured with equal exposure and gain settings, but the image contrast has been adjusted to present similar views.
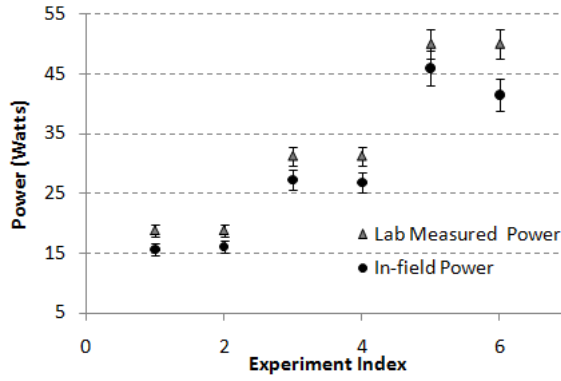
11

FIG. 5. Results of a field test of the scattered-light radiometric power meter. The triangles represent laser power as measured in a laboratory, and the dots are the power as measured by the camera. The difference between measured and expected power can be attributed to loss resulting from reflections in the beam director, aerosol scattering, and portions of the beam falling off the target in periods of high turbulence.
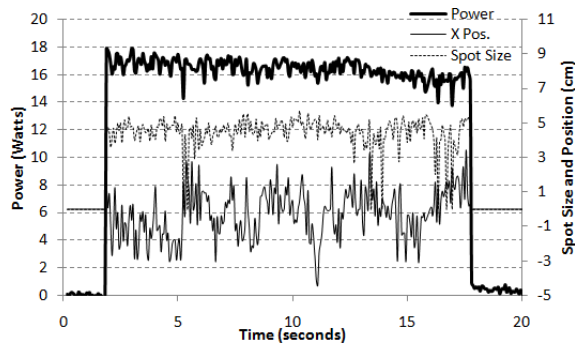

FIG. 6. A plot of the power P_o (thick line), spot radius (dotted line), and spot position (thin line) in the horizontal direction during the second run. The power fluctuations are produced by turbulence directing portions of the beam off of the target.

12